THE JOURNAL OF PHYSICAL CHEMISTRY B

pubs.acs.org/JPCB Article

Molecular Simulation of Covalent Bond Dynamics in Liquid Silicon

Published as part of The Journal of Physical Chemistry virtual special issue "Peter J. Rossky Festschrift".

Richard C. Remsing* and Michael L. Klein*

Cite This: *J. Phys. Chem. B* 2020, 124, 3180–3185 Read Online

ACCESS | Metrics & More | Article Recommendations

ABSTRACT: Many atomic liquids can form transient covalent bonds reminiscent of those in the corresponding solid states. These directional interactions dictate many important properties of the liquid state, necessitating a quantitative, atomic-scale understanding of bonding in these complex systems. A prototypical example is liquid silicon, wherein transient covalent bonds give rise to local tetrahedral order and consequent nontrivial effects on liquid-state thermodynamics and dynamics. To further understand covalent bonding in liquid silicon, and similar liquids, we present an ab initio-simulation-based approach for quantifying the structure and dynamics of covalent bonds in condensed phases. Through the examination of structural correlations among silicon nuclei and maximally localized Wannier function centers, we develop a geometric criterion for covalent bonds in liquid Si. We use this to monitor the dynamics of transient covalent bonding in the liquid state and estimate a covalent bond lifetime. We compare covalent bond dynamics to other processes in liquid Si and similar liquids and suggest experiments to measure the covalent bond lifetime.

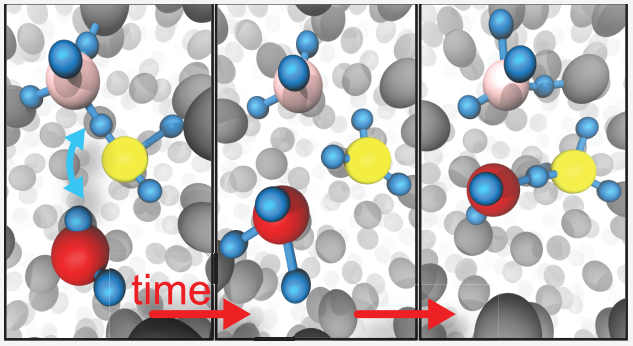

INTRODUCTION

Many metallic and semimetallic atomic liquids contain significant numbers of dynamic covalent bonds reminiscent of the static bonds formed in the corresponding solid state. The covalent bonds in these liquids are dynamic, readily breaking and forming on molecular time scales, and the characterization of these processes is complicated due to the interplay between electronic and nuclear structures. Such metallic liquids include molten silicon,[1−8] boron,[9] gallium,[10] and hydrogen at high pressure and temperature,[11−16] as well as many alloys, including those of importance in phase change random access memory materials.[17−19] These liquids play important roles in fuel cells, catalysis, and electrochemistry, where the dynamic covalent bonds are expected to play an important role in chemical reactivity.[20] Many of these liquids are also found in planetary cores,[16,21−25] and understanding their structure and dynamics is of importance to planetary and geophysical sciences.

In all of these fluids, a complete understanding of their properties requires knowledge of the fundamental interactions and time scales governing their chemical and physical transformations. The relative abundance of dynamic covalent bonds is expected to play a role in determining the thermodynamic properties of the liquid state, as well as the kinetics of phase transformations. For example, liquid silicon displays many of the hallmark anomalies found in water, because the covalent bonds in liquid silicon lead to tetrahedral structures, analogous to hydrogen bonding in water.

Due to the importance of silicon to the semiconductor industry and technology as a whole, *l*-Si is well-characterized. However, past research has mainly focused on the structure and thermodynamics of liquid silicon (*l*-Si). In the solid state under ambient conditions, silicon is a covalently bonded semiconductor in the diamond lattice, and upon melting, it undergoes a semiconductor-to-metal transition.[6,26−28] Early simulations indeed predicted that *l*-Si is metallic, in agreement with experiments, but they also uncovered a non-negligible fraction of covalent bonds that persist in the liquid state.[1−8] The existence of these remnants of the solid phase was later confirmed through a combination of computer simulations and Compton scattering experiments.[2]

The formation of covalent bonds in the disordered liquid state indicates the presence of a competition between metallic and covalent interactions in silicon. Indeed, a quantitative description of the solid phases of Si necessitates an accurate

Received: February 29, 2020
Revised: March 26, 2020
Published: March 27, 2020

https://dx.doi.org/10.1021/acs.jpcb.0c01798
J. Phys. Chem. B 2020, 124, 3180–3185

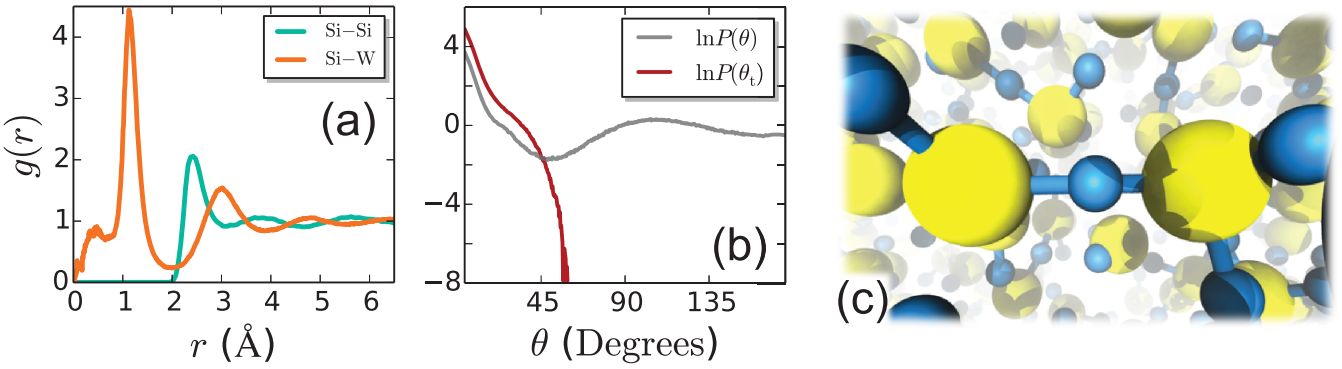

Figure 1. (a) Pair distribution functions, $g(r)$, for correlations between silicon nuclei (Si−Si) and between silicon atoms and maximally localized Wannier function centers (Si−W). (b) The natural logarithms of the probability distributions of the Si−Si−W angle (θ) and the Si−Si−W angle for triplets involving the additional constraint that the Si−W distance is within the largest peak in the Si−W $g(r)$, 0.75 Å < r_{Si-W} < 1.75 Å (θ_t). The probability distributions are normalized such that they equal unity for a uniform distribution. (c) Snapshot of a Si−Si covalent bond in liquid Si that satisfies the geometric definition proposed here. Si atoms are shown in yellow, and maximally localized Wannier function centers (W) are shown in blue.

model for the balance of metallic and covalent interatomic interactions.[6] This competition between metallic and covalent interactions is also predicted to underlie a metallic-to-semimetallic liquid−liquid phase transition in silicon.[5,8,29−31] In this case, a high density metallic *l*-Si that is dominated by metallic bonding can transition to a low density semimetallic liquid, in which the interatomic interactions are predominantly covalent bonds, albeit transient ones that readily break and reform in response to thermal fluctuations.[5,8,29−31]

Despite these significant investigations into the structure and thermodynamics of silicon, quantification of the lifetimes of the transient covalent bonds in *l*-Si is lacking. To address this issue, we use ab initio molecular dynamics (AIMD) simulations to characterize covalent bonding kinetics in *l*-Si, which serves as a prototypical liquid-state system with dynamic covalent bonds. After discussing simulation details in the next section, we quantify the structure of transient covalent bonds in *l*-Si and present a geometric covalent bond definition. We then use this definition to quantify the dynamics of covalent bonding in *l*-Si and conclude with a discussion of future directions.

SIMULATION DETAILS

We simulated liquid Si at T = 1800 K using the CP2K software package following our previous work.[8] The energies and forces in the MD simulations were evaluated using the *QUICKSTEP* module,[32,33] which employs basis sets of Gaussian-type orbitals and plane waves for the electron density. We used pseudopotentials, to represent the core electrons, and basis sets parametrized by Godecker−Teter−Hutter (GTH): GTH-PADE and GTH double-ζ, single polarization (GTH-DZVP), respectively.[33,34] We explicitly treated the valence electrons of the 216 Si atoms using the strongly constrained and appropriately normed (SCAN) meta-generalized gradient approximation (meta-GGA) density functional,[6,35] as implemented in LIBXC version 4.0.1,[36,37] with a plane wave cutoff of 650 Ry. Initial configurations were taken from extensively equilibrated simulations performed in earlier work.[7,8] The systems were then further equilibrated at a constant temperature of T = 1800 K, maintained using the canonical velocity rescaling thermostat.[38] Dynamic properties were computed from simulations in the microcanonical ensemble using a time step of 0.5 fs.

COVALENT BOND STRUCTURE IN LIQUID SILICON

We characterize the covalent bond structure in *l*-Si through the calculation of maximally localized Wannier functions (MLWFs) and their centers (MLWFCs).[39] MLWFs, in essence, can act as analogues of molecular orbitals for periodic systems, such as crystalline and amorphous solids and liquids, and provide a useful, local picture of chemical bonding.[39,40] We use the MLWFCs to represent the position of electrons, as done previously,[2,39−43] in order to quantify electron−nuclei correlations and develop a geometric criterion defining the existence of a covalent bond in an atomic configuration. We note that, although the MLWFs themselves are not unique, the MLWFCs are invariant with respect to the choice of gauge within a lattice vector, which is a time-independent constant for simulations in constant volume ensembles, like the microcanonical ensemble used here.[39,44] Thus, the MLWFCs can be used to define single bonds in each configuration.

We assume that covalent (single) bonds can be accurately defined by considering two- and three-body correlations among Si nuclei and MLWFCs (W). The relevant two-body correlations are encoded in pair distribution functions, $g(r)$, involving Si nuclei and MLWFCs. Three-body correlations are captured by the probability distributions $P(\theta)$, where θ is the Si−Si−MLWFC angle formed by an Si atom, its nearest neighbor Si atom, and a MLWFC. Both sets of distribution functions are shown in Figure 1.

The pair distribution functions for Si−Si and Si−MLWFC correlations, shown in Figure 1a, are consistent with the formation of covalent bonds between Si atoms. The first peak in the Si−W $g(r)$ is located halfway to the first Si−Si peak, and subsequent peaks in the two correlation functions are out of phase. Note that the small peak in the Si−W $g(r)$ at distances less than roughly 1 Å is consistent with the existence of nonbonded, lone pair electrons, visually depicted in Figure 4a−c.

Triplet correlations, as quantified by $P(\theta)$, show that a significant fraction of nearest-neighbor MLWFCs are consistent with covalent bonding, evidenced by the peak in $P(\theta)$ as θ approaches zero (Figure 1b), consistent with linear Si−MLWFC−Si arrangements. Large values of θ correspond to Si−Si−W triplets not involved in covalent bonds. We additionally consider the possibility that lone-pair-like MLWFCs may also appear at low values of θ. Thus, we place the additional constraint on the Si−Si−W angle that the Si−W distance must

https://dx.doi.org/10.1021/acs.jpcb.0c01798
J. Phys. Chem. B 2020, 124, 3180−3185

be between 0.75 and 1.75 Å to avoid counting lone pair MLWFCs, resulting in the angle θ_t. This more tightly constrained angle removes contributions from lone pairs to the angular distribution $P(\theta_t)$, Figure 1b. With this additional constraint, we suggest a reasonable geometric definition of a Si−Si covalent bond corresponds to a Si−Si distance less than 3 Å and $\theta_t < 30°$. One such covalent bond is highlighted in Figure 1c.

In the snapshot shown in Figure 1c as well as those in Figure 4a−c, one can observe a range of bonding and coordination environments. In particular, the number of MLWFCs associated with a single Si atom varies, and similarly, the number of Si atoms associated with a MLWFC also varies. Characterizing the fluctuations in Si and MLWFC coordination structures quantifies the probability of forming lone pairs, covalent bond pairs, and metallic or diffuse pairs.[2,9] However, positional correlations alone do not suffice to characterize the nature of the MLWFs, as discussed above in the context of angular correlations. Lone pairs and covalent bond MLWFs are highly localized in space, such that their spreads are small, and bonded MLWFs are generally more localized than lone pair MLWFs.[2,9] In contrast, the spreads of metallic or diffuse MLWFs are large, corresponding to delocalized pairs. Therefore, we quantify the coordination structure of Si atoms and MLWFCs through distances, as well as a range of MLWF spreads. We introduce a MLWF spread cutoff, σ_W, such that MLWFs with spreads above this value are not included in averages; $\sigma_W = \infty$ indicates that all MLWFCs are included in the calculations.

We start by examining the impact of σ_W on the Si−MLWFC pair distribution function, $g_{Si-W}(r)$, shown in Figure 2a.

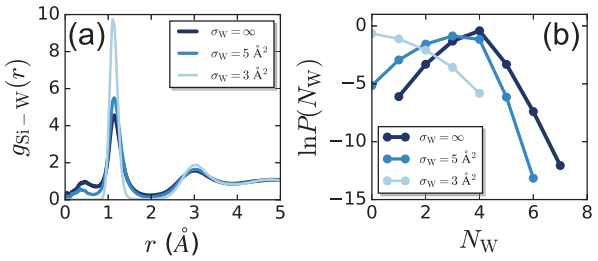

Figure 2. (a) Pair distribution functions, $g(r)$, for correlations between silicon nuclei and maximally localized Wannier function centers (Si−W) for indicated values of the cutoff for the spread of the MLWFs, σ_W, above which we exclude MLWFCs from the calculation. (b) Probability distributions, $P(N_W)$, of the number of MLWFCs, N_W, within a distance of 1.75 Å of a central Si atom for the same values of σ_W.

Introducing a finite σ_W removes the contribution of diffuse MLWFs from the pair distribution function. A spread cutoff of 5 Å^2 reduces the peak at small distances and slightly increases the first major peak, as well as the second peak. Further decreasing σ_W to 3 Å^2 removes diffuse and nearly all lone pairs, evidenced by an absence of a peak for $r < 1$ Å. The MLWFs remaining in the calculation are predominantly covalently bonded pairs, and the intensity of the first major peak in $g_{Si-W}(r)$, corresponding to bonded pairs, increases significantly. The second peak increases slightly as well. Therefore, σ_W can be tuned to remove diffuse and lone pair MLWFCs, and this tuning mainly impacts the structure of the first coordination shell, $r < 1.75$ Å.

The probabilities of observing N_W MLWFCs in the first coordination shell of a Si atom for various σ_W values are shown in Figure 2b. When all MLWFCs are included, N_W ranges from 1 to 7, and a maximum is observed at $N_W = 4$, as expected from the sp^3 hybridization of the Si atoms. As the cutoff is decreased, $P(N_W)$ shifts toward lower values, as delocalized MLWFs are removed from consideration. For $\sigma_W = 5$ Å^2, the maximum shifts to $N_W = 3$, with similar probabilities at $N_W = 2$ and $N_W = 4$. The appearance of finite probability for $N_W = 0$ is consistent with Si atoms that have all of their valence electrons in diffuse, metallic states. Further reduction of σ_W to 3 Å^2, which limits the set of MLWFCs almost entirely to covalently bonded pairs, shifts the maximum of $P(N_W)$ to zero, consistent with a small fraction (roughly 30%) of Si atoms involved in covalent bonds. In this limit, $P(N_W)$ essentially corresponds to the probability of a Si atom having N_W highly localized covalent bonds. This spans zero to four bonds per Si atom and monotonically decreases with N_W, indicating that Si atoms fully coordinated by covalent bonds are less probable than partially and nonbonded Si atoms. This is consistent with the metallic nature of liquid Si.

We now turn our attention to the coordination structure of the MLWFCs, particularly those that are in the first coordination shell of a Si atom. To quantify this, we compute the joint probability distribution, $P(N_{Si}, N_W)$, corresponding to the probability that a central Si atom is coordinated by N_W MLWFCs and one of those coordinated MLWFCs is in turn coordinated by N_{Si} Si atoms (including the central Si atom). A schematic for $N_W = 4$ and $N_{Si} = 2$ for one MLWFC is shown in Figure 3a. For ease of visualization, we focus on the conditional probability

$$P(N_{Si}|N_W) = \frac{P(N_{Si}, N_W)}{P(N_W)} \quad (1)$$

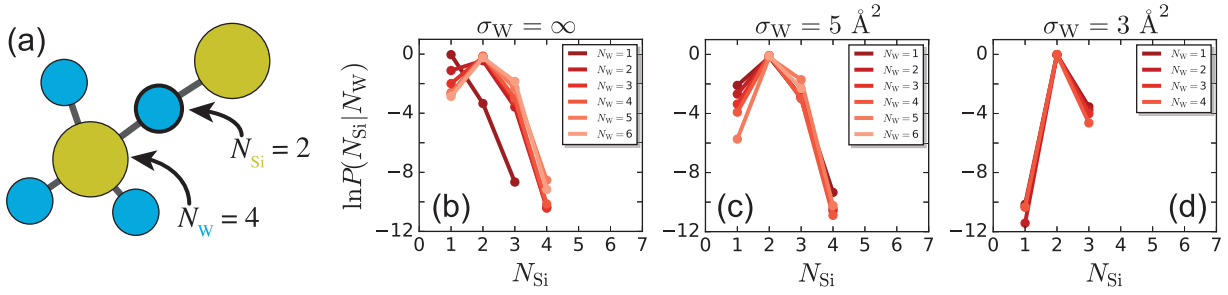

Figure 3. (a) Schematic diagram indicating the examples of N_W and the number of Si atoms around a MLWFC that is in the coordination shell of a Si atom, N_{Si}. Si atoms are colored yellow, and MLWFCs are colored blue. Arrows point toward the Si and MLWFC to which the indicated N_W and N_{Si} refer. (b−d) Conditional probability distributions, $P(N_{Si}|N_W)$, of the number of Si atoms within a distance of 1.75 Å of a MLWFC, where the MLWFC is part of a Si coordination shell composed of N_W MLWFCs, for the indicated values of the MLWFC spread cutoff, σ_W.

https://dx.doi.org/10.1021/acs.jpcb.0c01798
J. Phys. Chem. B 2020, 124, 3180−3185

physically corresponding to the probability that a MLWFC in the coordination shell of a central Si atom is coordinated by N_{Si} Si atoms, given that the central Si has N_W MLWFCs in its first coordination shell. These distributions are shown in Figure 3b,c for varying σ_W.

When all MLWFCs are included in $P(N_{Si}|N_W)$, the conditional probability has a maximum at $N_{Si} = 2$ for all values of $N_W > 1$. This maximum corresponds to a covalent bond between the central Si and a neighboring Si atom. Reducing N_W from 6 to 2 primarily impacts the probably of observing singly coordinated MLWFCs (to the central Si), which increases as N_W is lowered. For $N_W = 1$, $P(N_{Si}|N_W)$ differs significantly from the rest, with $N_{Si} = 1$ being most probable, indicating that the MLWFC is most likely a diffuse or lone pair.

Introducing a finite MLWF spread cutoff of $\sigma_W = 5$ Å^2 removes diffuse pairs and results in distributions that are similar for all N_{Si}, except $N_{Si} = 1$. As N_W is decreased, the probability of observing singly coordinated, lone pair MLWFCs increases. Further reduction of σ_W to 3 Å^2 results in sharp $P(N_{Si}|N_W)$ distributions that are nearly independent of N_W. These distributions span $1 \leq N_{Si} \leq 3$, with a large maximum at $N_{Si} = 2$, corresponding to covalent bond MLWFCs. We note that there is a small probability for lone pairs when $\sigma_W = 3$ Å^2, but lowering the spread cutoff further will increasingly remove these MLWFCs and select only covalently bonded pairs.[2,9]

In summary, the local (bonding) coordination structure of Si atoms significantly fluctuates and involves diffuse metallic, lone pair, and covalently bonded states. We have characterized these states, and the use of a MLWF spread cutoff, σ_W, can be used to systematically tune the involvement of these states when necessary. Alternatively, Si−Si−W angular correlations, in addition to Si−Si and Si−W distances, used in the above-described geometric definition of covalent bonds can be used to uncover covalently bonded MLWFCs in a similar manner, because linear Si−W−Si structures are consistent with $N_{Si} = 2$ covalently bonded pairs.

COVALENT BOND DYNAMICS IN LIQUID SILICON

Our simulations suggest that covalent bonds in *l*-Si rapidly break and reform on sub-picosecond time scales. Parts a−c of Figure 4 highlight one such covalent bond breakage and reformation event. There, we show the time evolution of the MLWFCs (blue spheres) for the atoms involved in the highlighted covalent bond exchange. Initially (a), the central yellow Si atom is bonded to the left pink Si atom; a linear Si−MLWFC−Si structure indicates a single covalent bond expected from the sp^3 hybridization of Si. This bond breaks at a later time (b) due to thermal fluctuations, before the MLWFC of the central Si rotates and forms a new bond with the rightmost red Si (c).

Using the geometric definition of a covalent bond described in the previous section, we are able to quantify the kinetics of Si−Si bond breakage, in a manner analogous to conventional approaches to characterizing hydrogen bond dynamics in water,[45−47] and, more recently, halogen bond dynamics in solid and liquid chlorine.[41,43] To do so, we define an indicator function, $h(t)$, which is equal to 1 when a covalent bond is present and zero otherwise. We quantify covalent bond kinetics through the reactive flux correlation function[45]

$$k(t) = -\frac{dC(t)}{dt} = -\frac{\langle \dot{h}(0)[1 - h(t)]\rangle}{\langle h\rangle} \quad (2)$$

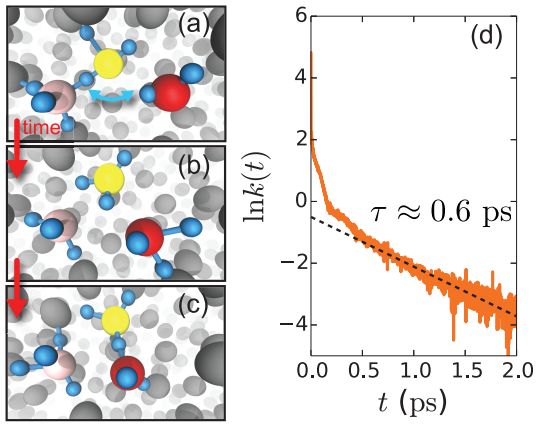

Figure 4. (a−c) Snapshots of covalent bond breakage and reformation in liquid silicon, with three Si atoms involved in the events colored yellow, pink, and red; all other Si atoms are colored gray. Maximally localized Wannier function centers (MLWFCs) associated with the colored silicon atoms are shown in blue. (a) Initially, the central (yellow) Si is bonded to the pink Si atom on the left, as indicated by the lines connecting the Si atoms through a bridging MLWFC. (b) At some time later, the bond breaks due to thermal fluctuations, and the MLWFC does not connect to Si atoms. (c) A new bond then forms between the central Si atom and the rightmost (red) colored Si atom. The left (pink) Si has also formed a new bond on this time scale. (d) The kinetics of bond covalent bond breakage is quantified by the reactive flux correlation function, $k(t)$, and fitting its long time behavior (dashed line) results in a covalent bond lifetime of $\tau \approx 0.6$ ps.

where $C(t)$ is the time correlation function (TCF) characterizing covalent bond lifetimes

$$C(t) = \frac{\langle h(t)h(0)\rangle}{\langle h\rangle} \quad (3)$$

The reactive flux correlation function, $k(t)$, is shown in Figure 4d. At short times, vibrational and librational motion manifest the nontrivial, transient behavior on scales less than roughly 0.3 ps. Beyond this time period, $k(t)$ decays in a manner consistent with first-order kinetics, $k(t) \sim \tau^{-1} \exp(t/\tau)$, where $\tau \approx 0.6$ ps is the covalent bond lifetime estimated from fitting to the long-time behavior of $k(t)$, shown as a dashed line in Figure 4d.

The covalent bond lifetime estimated above is similar to other significant time scales in *l*-Si. Orientational correlations, the velocity autocorrelation function, and self-intermediate scattering functions all decay on time scales similar to the covalent bond lifetime.[7,8] The agreement among various structural relaxation times and the covalent bond lifetime suggests that covalent bond breakage is a limiting step for structural relaxation. This may be expected from the strength of covalent bonds, as well as their propensity to create local tetrahedral order in the liquid state.

CONCLUSIONS

In this work, we have presented an approach to estimate the lifetimes of transient covalent bonds in condensed phase systems with an application to liquid silicon. The general strategy utilizes a maximally localized Wannier function (MLWF) approach to chemical bonding, such that the existence of a covalent bond can be defined using two-body Si−Si correlations and three-body correlations involving two Si nuclei and the center of a MLWF. With this geometric, ab initio definition of a covalent bond, we can estimate covalent bond lifetimes in the liquid state from

https://dx.doi.org/10.1021/acs.jpcb.0c01798
J. Phys. Chem. B 2020, 124, 3180−3185

equilibrium simulations using the reactive flux formalism. For liquid silicon at 1800 K and ambient pressure, we estimate a covalent bond lifetime of $\tau \approx 0.6$ ps. We note, however, that the generic concept of monitoring bond dynamics using a geometric, electronic-structure-based bond definition is not limited to equilibrium and could be used to monitor covalent bond dynamics in melting or freezing processes at the focus of laster melting experiments,[30,48,49] for example.

The covalent bond lifetime in liquid silicon may be measured using time-dependent scattering measurements, such as a time-dependent Compton scattering. Compton scattering has been used to shed light on the average bonding properties of metallic liquids.[2,9] Extensions of this technique to the time domain are expected to uncover similar information about the average dynamic properties of transient covalent bonds, like the lifetime at the focus of this work.[50−52]

Finally, we note that the covalent bond lifetime in *l*-Si is similar to bond lifetimes in other conventional liquids with directional attractive interactions. The hydrogen bond lifetime in liquid water is on the picosecond time scale,[46,47] as is the halogen bond lifetime in liquid Cl_2.[41] Despite the vast differences in these liquids, their directional bonds all share a common thread: the strength of the isolated bond, which is significantly weakened in the condensed phase, is on the order of $10k_BT$ at the temperature of the respective liquids.[53] Thus, thermal fluctuations in each of these different liquids are large enough to cause the directional attractions to exist only fleetingly, highlighting qualitative similarities of directional bond dynamics in the liquid state.

AUTHOR INFORMATION

Corresponding Authors

Richard C. Remsing − *Department of Chemistry and Chemical Biology, Rutgers University, Piscataway, New Jersey 08854, United States;* orcid.org/0000-0002-0922-4882; Email: rick.remsing@rutgers.edu

Michael L. Klein − *Institute for Computational Molecular Science and Department of Chemistry, Temple University, Philadelphia, Pennsylvania 19122, United States;* Email: mlklein@temple.edu

Complete contact information is available at: https://pubs.acs.org/10.1021/acs.jpcb.0c01798

Notes

The authors declare no competing financial interest.

ACKNOWLEDGMENTS

This work was supported as part of the Center for Complex Materials from First-Principles (CCM), an Energy Frontier Research Center funded by the U.S. Department of Energy, Office of Science, Basic Energy Sciences under award no. DE-SC0012575. Computational resources were supported in part by the National Science Foundation through major research instrumentation grant no. 1625061 and by the US ARL under contract no. W911NF-16-2-0189.

REFERENCES

(1) Štich, I.; Car, R.; Parrinello, M. Structural, bonding, dynamical, and electronic properties of liquid silicon: An *ab initio* molecular-dynamics study. *Phys. Rev. B: Condens. Matter Mater. Phys.* **1991**, *44*, 4262−4274.

(2) Okada, J. T.; Sit, P. H.-L.; Watanabe, Y.; Wang, Y. J.; Barbiellini, B.; Ishikawa, T.; Itou, M.; Sakurai, Y.; Bansil, A.; Ishikawa, R.; et al. Persistence of covalent bonding in liquid silicon probed by inelastic x-ray scattering. *Phys. Rev. Lett.* **2012**, *108*, 067402.

(3) Štich, I.; Parrinello, M.; Holender, J. M. Dynamics, Spin Fluctuations, and Bonding in Liquid Silicon. *Phys. Rev. Lett.* **1996**, *76*, 2077−2080.

(4) Štich, I.; Car, R.; Parrinello, M. Bonding and Disorder in Liquid Silicon. *Phys. Rev. Lett.* **1989**, *63*, 2240−2243.

(5) Ashwin, S. S.; Waghmare, U. V.; Sastry, S. Metal-to-semimetal transition in supercooled liquid silicon. *Phys. Rev. Lett.* **2004**, *92*, 175701.

(6) Sun, J.; Remsing, R. C.; Zhang, Y.; Sun, Z.; Ruzsinszky, A.; Peng, H.; Yang, Z.; Paul, A.; Waghmare, U.; Wu, X.; et al. Accurate first-principles structures and energies of diversely bonded systems from an efficient density functional. *Nat. Chem.* **2016**, *8*, 831−6.

(7) Remsing, R. C.; Klein, M. L.; Sun, J. Dependence of the structure and dynamics of liquid silicon on choice of density functional approximation. *Phys. Rev. B: Condens. Matter Mater. Phys.* **2017**, *96*, 024203.

(8) Remsing, R. C.; Klein, M. L.; Sun, J. Refined description of liquid and supercooled silicon from ab initio simulations. *Phys. Rev. B: Condens. Matter Mater. Phys.* **2018**, *97*, No. 140103.

(9) Okada, J.; Sit, P.-L.; Watanabe, Y.; Barbiellini, B.; Ishikawa, T.; Wang, Y.; Itou, M.; Sakurai, Y.; Bansil, A.; Ishikawa, R.; et al. Visualizing the Mixed Bonding Properties of Liquid Boron with High-Resolution X-Ray Compton Scattering. *Phys. Rev. Lett.* **2015**, *114*, 177401.

(10) Gong, X. G.; Chiarotti, G. L.; Parrinello, M.; Tosatti, E. Coexistence of Monatomic and Diatomic Molecular Fluid Character in Liquid Gallium. *Europhys. Lett.* **1993**, *21*, 469−475.

(11) Rillo, G.; Morales, M. A.; Ceperley, D. M.; Pierleoni, C. Optical properties of high-pressure fluid hydrogen across molecular dissociation. *Proc. Natl. Acad. Sci. U. S. A.* **2019**, *116*, 9770−9774.

(12) Morales, M. A.; McMahon, J. M.; Pierleoni, C.; Ceperley, D. M. Nuclear Quantum Effects and Nonlocal Exchange-Correlation Functionals Applied to Liquid Hydrogen at High Pressure. *Phys. Rev. Lett.* **2013**, *110*, 065702.

(13) Pierleoni, C.; Holzmann, M.; Ceperley, D. M. Local structure in dense hydrogen at the liquid-liquid phase transition by coupled electron-ion Monte Carlo. *Contrib. Plasma Phys.* **2018**, *58*, 99−106.

(14) Pierleoni, C.; Morales, M. A.; Rillo, G.; Holzmann, M.; Ceperley, D. M. Liquid−liquid phase transition in hydrogen by coupled electron−ion Monte Carlo simulations. *Proc. Natl. Acad. Sci. U. S. A.* **2016**, *113*, 4953−4957.

(15) Pierleoni, C.; Rillo, G.; Ceperley, D. M.; Holzmann, M. Electron localization properties in high pressure hydrogen at the liquid-liquid phase transition by Coupled Electron-Ion Monte Carlo. *J. Phys.: Conf. Ser.* **2018**, *1136*, 012005.

(16) Zaghoo, M.; Silvera, I. F. Conductivity and dissociation in liquid metallic hydrogen and implications for planetary interiors. *Proc. Natl. Acad. Sci. U. S. A.* **2017**, *114*, 11873−11877.

(17) Lee, T. H.; Elliott, S. R. The Relation between Chemical Bonding and Ultrafast Crystal Growth. *Adv. Mater.* **2017**, *29*, 1700814.

(18) Loke, D.; Lee, T. H.; Wang, W. J.; Shi, L. P.; Zhao, R.; Yeo, Y. C.; Chong, T. C.; Elliott, S. R. Breaking the Speed Limits of Phase-Change Memory. *Science* **2012**, *336*, 1566−1569.

(19) Skelton, J. M.; Loke, D.; Lee, T.; Elliott, S. R. Ab Initio Molecular-Dynamics Simulation of Neuromorphic Computing in Phase-Change Memory Materials. *ACS Appl. Mater. Interfaces* **2015**, *7*, 14223−14230.

(20) Zavabeti, A.; Ou, J. Z.; Carey, B. J.; Syed, N.; Orrell-Trigg, R.; Mayes, E. L. H.; Xu, C.; Kavehei, O.; O'Mullane, A. P.; Kaner, R. B.; et al. A liquid metal reaction environment for the room-temperature synthesis of atomically thin metal oxides. *Science* **2017**, *358*, 332−335.

(21) Poirier, J.-P. Light elements in Earth's outer core: A critical review. *Phys. Earth Planet. Inter.* **1994**, *85*, 319−337.

(22) Pozzo, M.; Davies, C.; Gubbins, D.; Alfè, D. Transport properties for liquid silicon-oxygen-iron mixtures at Earth's core conditions. *Phys. Rev. B: Condens. Matter Mater. Phys.* **2013**, *87*, 014110.

(23) Pozzo, M.; Davies, C.; Gubbins, D.; Alfè, D. Thermal and electrical conductivity of solid iron and iron-silicon mixtures at Earth's core conditions. *Earth Planet. Sci. Lett.* **2014**, *393*, 159−164.

(24) Williams, Q. The Thermal Conductivity of Earth's Core: A Key Geophysical Parameter's Constraints and Uncertainties. *Annu. Rev. Earth Planet. Sci.* **2018**, *46*, 47−66.
(25) Mazzola, G.; Helled, R.; Sorella, S. Phase Diagram of Hydrogen and a Hydrogen-Helium Mixture at Planetary Conditions by Quantum Monte Carlo Simulations. *Phys. Rev. Lett.* **2018**, *120*, 025701.
(26) Sugino, O.; Car, R. *Ab Initio* Molecular Dynamics Study of First-Order Phase Transitions: Melting of Silicon. *Phys. Rev. Lett.* **1995**, *74*, 1823−1826.
(27) Alfè, D.; Gillan, M. J. Exchange-correlation energy and the phase diagram of Si. *Phys. Rev. B: Condens. Matter Mater. Phys.* **2003**, *68*, 205212.
(28) McMillan, P. F.; Wilson, M.; Daisenberger, D.; Machon, D. A density-driven phase transition between semiconducting and metallic polyamorphs of silicon. *Nat. Mater.* **2005**, *4*, 680−4.
(29) Ganesh, P.; Widom, M. Liquid-liquid transition in supercooled silicon determined by first-principles simulation. *Phys. Rev. Lett.* **2009**, *102*, 075701.
(30) Beye, M.; Sorgenfrei, F.; Schlotter, W. F.; Wurth, W.; Föhlisch, A. The liquid-liquid phase transition in silicon revealed by snapshots of valence electrons. *Proc. Natl. Acad. Sci. U. S. A.* **2010**, *107*, 16772−6.
(31) Sastry, S. Illuminating liquid polymorphism in silicon. *Proc. Natl. Acad. Sci. U. S. A.* **2010**, *107*, 17063−4.
(32) VandeVondele, J.; Krack, M.; Mohamed, F.; Parrinello, M.; Chassaing, T.; Hutter, J. QUICKSTEP: Fast and Accurate Density Functional Calculations Using a Mixed Gaussian and Plane Waves Approach. *Comput. Phys. Commun.* **2005**, *167*, 103−128.
(33) VandeVondele, J.; Hutter, J. Gaussian Basis Sets for Accurate Calculations on Molecular Systems in Gas and Condensed Phases. *J. Chem. Phys.* **2007**, *127*, 114105.
(34) Goedecker, S.; Teter, M.; Hutter, J. Separable Dual-Space Gaussian Pseudopotentials. *Phys. Rev. B: Condens. Matter Mater. Phys.* **1996**, *54*, 1703−1710.
(35) Sun, J.; Ruzsinszky, A.; Perdew, J. P. Strongly Constrained and Appropriately Normed Semilocal Density Functional. *Phys. Rev. Lett.* **2015**, *115*, 036402.
(36) Lehtola, S.; Steigemann, C.; Oliveira, M. J.; Marques, M. A. Recent developments in libxc — A comprehensive library of functionals for density functional theory. *SoftwareX* **2018**, *7*, 1−5.
(37) Marques, M. A.; Oliveira, M. J.; Burnus, T. Libxc: A library of exchange and correlation functionals for density functional theory. *Comput. Phys. Commun.* **2012**, *183*, 2272−2281.
(38) Bussi, G.; Donadio, D.; Parrinello, M. Canonical sampling through velocity rescaling. *J. Chem. Phys.* **2007**, *126*, 014101.
(39) Marzari, N.; Mostofi, A. A.; Yates, J. R.; Souza, I.; Vanderbilt, D. Maximally Localized Wannier Functions: Theory and Applications. *Rev. Mod. Phys.* **2012**, *84*, 1419−1475.
(40) Silvestrelli, P. L.; Marzari, N.; Vanderbilt, D.; Parrinello, M. Maximally-Localized Wannier Functions for Disordered Systems: Application to Amorphous Silicon. *Solid State Commun.* **1998**, *107*, 7−11.
(41) Remsing, R. C.; Klein, M. L. Halogen Bond Structure and Dynamics from Molecular Simulations. *J. Phys. Chem. B* **2019**, *123*, 6266−6273.
(42) Remsing, R. C.; Sun, J.; Waghmare, U. V.; Klein, M. L. Bonding in the Metallic Molecular Solid α-Gallium. *Mol. Phys.* **2018**, *116*, 3372−3379.
(43) Remsing, R. C.; Klein, M. L. Lone Pair Rotational Dynamics in Solids. *Phys. Rev. Lett.* **2020**, *124*, 066001.
(44) Blount, E. *Solid state physics*; Elsevier: 1962; Vol. *13*, pp 305−373.
(45) Chandler, D. Statistical mechanics of isomerization dynamics in liquids and the transition state approximation. *J. Chem. Phys.* **1978**, *68*, 2959−2970.
(46) Luzar, A. Resolving the Hydrogen Bond Dynamics Conundrum. *J. Chem. Phys.* **2000**, *113*, 10663−10675.
(47) Luzar, A.; Chandler, D. Hydrogen-Bond Kinetics in Liquid Water. *Nature* **1996**, *379*, 55−57.
(48) Stiffler, S. R.; Thompson, M. O.; Peercy, P. S. Supercooling and Nucleation of Silicon after Laser Melting. *Phys. Rev. Lett.* **1988**, *60*, 2519−2522.
(49) Sanders, P. G.; Aziz, M. J. Self-diffusivity of liquid silicon measured by pulsed laser melting. *J. Appl. Phys.* **1999**, *86*, 4258−4261.
(50) Wagner, R. E.; Su, Q.; Grobe, R. Time-resolved Compton scattering for a model fermion-boson system. *Phys. Rev. A: At., Mol., Opt. Phys.* **2010**, *82*, 022719.
(51) Kemper, A. F.; Sentef, M.; Moritz, B.; Kao, C. C.; Shen, Z. X.; Freericks, J. K.; Devereaux, T. P. Mapping of unoccupied states and relevant bosonic modes via the time-dependent momentum distribution. *Phys. Rev. B: Condens. Matter Mater. Phys.* **2013**, *87*, 235139.
(52) Grosser, M.; Slowik, J. M.; Santra, R. Attosecond x-ray scattering from a particle-hole wave packet. *Phys. Rev. A: At., Mol., Opt. Phys.* **2017**, *95*, 062107.
(53) Bryant, R. G.; Johnson, M. A.; Rossky, P. J. Water. *Acc. Chem. Res.* **2012**, *45*, 1−2.

https://dx.doi.org/10.1021/acs.jpcb.0c01798
J. Phys. Chem. B 2020, 124, 3180−3185